

WANG, S., WU, F., TAKYI-ANINAKWA, P., FERNANDEZ, C., STROE, D.-I. and HUANG, Q. 2023. Improved singular filtering-Gaussian process regression-long short-term memory model for whole-life-cycle remaining capacity estimation of lithium-ion batteries adaptive to fast aging and multi-current variations. *Energy* [online], 284, article 128677. Available from: <https://doi.org/10.1016/j.energy.2023.128677>

# Improved singular filtering-Gaussian process regression-long short-term memory model for whole-life-cycle remaining capacity estimation of lithium-ion batteries adaptive to fast aging and multi-current variations.

WANG, S., WU, F., TAKYI-ANINAKWA, P., FERNANDEZ, C., STROE, D.-I.  
and HUANG, Q.

2023

# Energy

## Improved singular filtering-Gaussian regression-long short-term memory network for whole-life-cycle remaining capacity prediction of lithium-ion batteries adaptive to fast-charge aging and multiple current variations

--Manuscript Draft--

<b>Manuscript Number:</b>	EGY-D-22-05258R1
<b>Article Type:</b>	Full length article
<b>Keywords:</b>	lithium-ion battery; singular filtering-Gaussian regression-long short-term memory network; whole-life-cycle remaining capacity prediction; fast-fading aging; Collaborative carrier transport
<b>Corresponding Author:</b>	Shunli Wang, Prof.Dr.  Mianyang, CHINA
<b>First Author:</b>	Shunli Wang, Prof.Dr.
<b>Order of Authors:</b>	Shunli Wang, Prof.Dr. Fan Wu Paul Takyi-Aninakwa, Dr. Carlos Fernandez, Prof.Dr. Daniel-loan Stroe, Prof.Dr. Qi Huang, Prof.Dr.
<b>Abstract:</b>	<p>For the development of low-temperature power systems in aviation, the transport synergistic carrier optimization of lithium-ions and electrons is conducted to improve the low-temperature adaptability of lithium-ion batteries. In this paper, an improved robust multi-time scale singular filtering-Gaussian process regression-long short-term memory (SF-GPR-LSTM) modeling method is proposed for the remaining capacity estimation. The optimized multi-task training strategy is constructed for the rapid battery performance evaluation, realizing the refined mathematical dynamic characterization for the mapping relationship of the physical carrier transports to obtain the simultaneous improvement of multi-dimensional physical features and a spiral-up iterative optimization scheme. The adaptability of the model is verified using datasets from the whole-life-cycle test conducted on two batteries, and evaluated by root mean squared error (RMSE), mean absolute error (MAE), mean absolute percentage error (MAPE), and R-squared metrics. Even when only using 55% of the datasets to estimate the remaining capacity, the estimation has good effects, with RMSE of 2.3484%, MAE of 0.82526%, MAPE of 0.90716%, and R-squared value of 92.457%. The proposed SF-GPR-LSTM model enables the carrier transport synergistic optimization effectively, laying a theoretical foundation for the whole-life-cycle battery remaining capacity estimation at extremely low temperatures.</p>

# Improved singular filtering-Gaussian process regression-long short-term memory model for whole-life-cycle remaining capacity estimation of lithium-ion batteries adaptive to fast aging and multi-current variations

Shunli Wang<sup>1,2\*</sup>, Fan Wu<sup>1</sup>, Paul Takyi-Aninakwa<sup>1</sup>, Carlos Fernandez<sup>4</sup>, Daniel-Ioan Stroe<sup>3</sup>, Qi Huang<sup>1</sup>

<sup>1</sup>School of Information Engineering, Southwest University of Science and Technology, Mianyang 621010, China; <sup>2</sup>College of Electrical Engineering,

Sichuan University, Chengdu 610065, China; <sup>3</sup>Department of Energy Technology, Aalborg University, Pontoppidanstraede 111 9220 Aalborg East,

Denmark; <sup>4</sup>School of Pharmacy and Life Sciences, Robert Gordon University, Aberdeen AB10-7GJ, UK.

**Abstract:** For the development of low-temperature power systems in aviation, the transport synergistic carrier optimization of lithium-ions and electrons is conducted to improve the low-temperature adaptability of lithium-ion batteries. In this paper, an improved robust multi-time scale singular filtering-Gaussian process regression-long short-term memory (SF-GPR-LSTM) modeling method is proposed for the remaining capacity estimation. The optimized multi-task training strategy is constructed for the rapid battery performance evaluation, realizing the refined mathematical dynamic characterization for the mapping relationship of the physical carrier transports to obtain the simultaneous improvement of multi-dimensional physical features and a spiral-up iterative optimization scheme. The adaptability of the model is verified using datasets from the whole-life-cycle test conducted on two batteries, and evaluated by root mean squared error (RMSE), mean absolute error (MAE), mean absolute percentage error (MAPE), and R-squared metrics. Even when only using 55% of the datasets to estimate the remaining capacity, the estimation has good effects, with RMSE of 2.3484%, MAE of 0.82526%, MAPE of 0.90716%, and R-squared value of 92.457%. The proposed SF-GPR-LSTM model enables the carrier transport synergistic optimization effectively, laying a theoretical foundation for the whole-life-cycle battery remaining capacity estimation at extremely low temperatures.

**Keywords:** lithium-ion battery; singular filtering-Gaussian process regression-long short-term memory network; whole-life-cycle remaining capacity estimation; fast-fading aging; collaborative carrier transport

\*Corresponding author: Shunli Wang. E-mail address: wangshunli@swust.edu.cn.

## Highlights:

- An improved SF-GPR-LSTM model is designed for remaining capacity estimation.
- The robust capacity estimation method is adaptive to low-temperature conditions.
- Multi-task training and optimization are conducted for the whole-life-cycle estimation.
- Real-time correction is realized for time-varying characterization and calculation.
- Coordinated transport optimization is carried out for the feature spiral-up strategy.

## Abbreviation-symbol set:

Nomenclature	Full name	Nomenclature	Full name
SF	singular filtering	$h_t$	hidden state or the learning output
GPR	Gaussian process regression	$f_t$	forget gate
LSTM	long short-term memory	$i_t$	input gate
RMSE	root mean squared error	$O_t$	output gate
MAE	mean absolute error	$\sigma$	sigmoid activate function
MAPE	mean absolute percentage error	$W$	weight matrix attached to each gate
SEI	solid electrolyte interface	$b$	bias vectors attached to each gate
SVR	support vector regression	$W_f$	weight attached to the forget gate
DL	deep learning	$b_f$	bias vector attached to the forget gate
RNN	recurrent neural network	$h_{t-1}$	previous hidden state
$\mu$	mobility of lithium-ions	$W_i/W_c$	weight coefficient
$\eta$	viscosity of electrolytes	$b_i$	corresponding bias vectors attached to the input gate
$r$	radius of the lithium-ion	$b_c$	corresponding bias vectors attached to the cell state
EC	ethylene carbonate	$C_t$	cell state information at time point $t$
DC	dimethyl carbonate	$W_o$	weight to the output gate
DC	diethyl carbonate	$b_o$	bias vector attached to the output gate
EA	ethyl acetate	$\vec{h}$	hidden layer stores the vector
DCM	dichloromethane	$\bar{h}$	forwarding estimation and the vector
LMO	lithium-ion manganese oxide	$y_t$	final output result
$x_t$	input data sequence	W10	filtering window with a width of 10

## 1. Introduction

The adaptation of lithium-ion batteries to the low-temperature environment in the aviation field is essential. In the lunar shadow area, the ambient operating temperature can be as low as  $-160\text{ }^\circ\text{C}$ . For modern equipment, to ensure its effectiveness and rapid response capability under all climatic conditions, the battery requires a reliable power output capacity at a low temperature of  $-55\text{ }^\circ\text{C}$ . After testing, there is a sharp decline in the discharge capacity, power state, and cycle life of the existing lithium-ion batteries under low-temperature conditions. It results in huge volume and weight overhead, which affects

1  
2 the reliability of the equipment enormously. Therefore, it is of great significance in guiding the research and development of  
3  
4 low-temperature lithium-ion batteries to quickly judge the performance under rapid attenuation at low temperatures and  
5  
6 realize targeted optimization.

7  
8 The energy conversion mechanism of lithium-ion batteries involves the multi-stage carrier transport process of the  
9  
10 components, including the cathode, anode, and electrolyte [1]. The ambient temperature and other environmental factors play  
11  
12 a vital role in the operation and performance of these components. For the cathode, the low temperature and the intrinsic  
13  
14 dynamic hysteresis are the fundamental reasons for the deterioration of carrier transport performance at 2–3 times the speed  
15  
16 [2-4]. For the anode, extremely low-temperature conditions increase the internal resistance of the solid electrolyte interface  
17  
18 (SEI) layer and reduce the lithium-ion diffusion coefficient magnitude [5]. For the electrolyte, low temperature is a significant  
19  
20 cause of the increase in solvent viscosity and the decrease in solid-liquid interfaces and infiltration characteristics [6]. It  
21  
22 makes the lithium-ion migration deteriorate significantly, which is the main link leading to the electrolyte and electrode  
23  
24 attenuation of lithium-ion batteries at extremely low temperatures [7-9]. Therefore, optimizing the physical properties and  
25  
26 regulating the transport characteristics of carriers for the ions and electrons are effective means to improve the low-  
27  
28 temperature performance of lithium-ion batteries [10]. However, the low-temperature performance improvement is limited  
29  
30 if it is only optimized by a single electrolyte, electrode, or interface control method, which is difficult to do so for lithium-  
31  
32 ion batteries [11-13]. Therefore, to realize the high-efficiency energy supply of lithium-ion batteries at low temperatures, it  
33  
34 is necessary to carry out the coordinated optimization of carrier transport in the cathode, anode, electrolyte, and corresponding  
35  
36 SEI layer.

37  
38 For the optimization goal of collaborative adaptive transport to low-temperature reduction and the quick battery  
39  
40 performance judgment has the guiding significance of adjusting the material synthesis parameters [14-16]. The existing  
41  
42 experimental testing method has a long iterative cycle and limited performance characteristics. It takes more than six months  
43  
44 from material research and development to battery preparation and performance testing, which significantly affects the  
45  
46 efficiency of carrier cooperative transport optimization [17-19]. Generally, the means to improve the performance of batteries  
47  
48  
49  
50  
51  
52  
53  
54  
55  
56  
57  
58  
59  
60  
61

at low temperatures mainly includes two aspects. One means is to improve the carrier transport process by accurately modeling the adaptability of the battery to low-temperature conditions. The second means is to adopt effective thermal management to ensure that the battery works at appropriate temperature conditions [20]. Adverse factors are introduced for the additional energy consumption, volume increases, and complex management in the thermal management scheme. The modeling-based method has the advantages of fast aging, high-throughput verification, and multi-feature parameter characterization [21]. However, the existing models have not fully considered the performance degradation characteristics caused by the low-temperature conditions. There are some problems in the realization processes, such as the incomplete acquisition of characteristic information, incomplete description of the carrier transport process, and complex coupling relationship characterization [22-24]. The composite electrochemical-thermal circuit model can directly measure the difficulty of electron and lithium-ion transfer to the electrodes and electrolyte by considering temperature and hysteresis effects.

Developing a carrier transport optimization strategy matching extremely low temperatures is a fundamental way to solve the performance degradation of lithium-ion batteries. Breaking the bottlenecks for low-temperature battery performance improvement through material design [25]. The optimal design of the electrolyte is realized for -55 °C or even lower temperature conditions. Then, the low-temperature dynamic characteristics of solid ion transport in the cathode and anode are improved [26]. Lots of research and repeated iterative optimization are carried out continuously. The main factors restricting the low-temperature performance of lithium-ion batteries include the decrease in Li<sup>+</sup> migration rate and conductivity, the increase of electrolyte or positive and negative interface impedance [27]. According to the Stokes-Einstein equation for diffusion, the mathematical relationship is obtained as  $\mu = 1/6\pi\eta r$ .  $\mu$  represents the mobility of lithium-ions,  $\eta$  represents the viscosity of electrolytes, and  $r$  represents the radius of the lithium-ion solvation shell. The transportation of lithium-ions in the electrolyte is mainly affected by two factors, including the viscosity of the electrolyte and the solvation structure around lithium-ions [28]. However, the viscosity of the electrolyte and the solvation structure around lithium-ions vary with temperature [29]. Therefore, a key to improving the transport characteristics of lithium-ions from the perspective

of electrolytes is to regulate the viscosity of electrolytes and the solvation structure around lithium-ions at low temperatures.

1  
2 Choosing an electrolyte solvent with a low viscosity and melting point is an effective way to improve the viscosity increase  
3  
4 of electrolytes at low temperatures. Researchers from the US Army laboratory have developed a series of lithium-ion battery  
5  
6 electrolytes with a low melting point, such as ethylene carbonate (EC), dimethyl carbonate (DMC), and diethyl carbonate (DEC)  
7  
8 battery chemistry [30]. The viscosity of the electrolyte used reduces at low temperatures and improves the internal resistance  
9  
10 of charge transfer on the graphite surface [31]. In addition to the combination of the above traditional organic solvents, ethyl  
11  
12 acetate (EA), a solvent with an ultra-low melting point (-84 °C) and dichloromethane (DCM), whose viscosity is only 0.44  
13  
14 MPa at -95 °C, are currently the research hotspots of low-temperature electrolytes [32]. A new electrolyte of 5 m LiTFSI/EA  
15  
16 + DCM (V: V, 1:4) is prepared, which still has a high lithium-ion conductivity of 0.6 mS $\text{cm}^{-1}$ , and a low electrolyte viscosity  
17  
18 of 0.35 MPas even at -70 °C [33]. In addition to regulating the viscosity of electrolytes, the solvation and desolvation behavior  
19  
20 of lithium-ions is also a key factor affecting the rapid transport of lithium-ions in low-temperature conditions [34]. A  
21  
22 LiTFSI/ethyl trifluoroacetate electrolyte is constructed with a low melting point (ETFA, melting point of -78 °C). Molecular  
23  
24 dynamics calculations showed that the binding energy between Li<sup>+</sup>-ETFA is only 10.05 kJmol<sup>-1</sup>, which is less than that of  
25  
26 conventional Li<sup>+</sup>-EC, EA, and DMC using 21.56, 28.18, and 19.07 kJmol<sup>-1</sup>, respectively [35]. This result shows that the  
27  
28 desolvation process of Li<sup>+</sup>-ETFA in low-temperature conditions is easier than in traditional Li<sup>+</sup>-carbonate solvents, and it is  
29  
30 easier to obtain higher lithium-ion mobility.  
31  
32  
33  
34  
35  
36  
37  
38  
39  
40  
41  
42

43 As the central site of electron and ion transfer, the cathode material is also the core link affecting the low-temperature  
44  
45 performance of lithium-ion batteries. The decrease in temperature significantly affects the reaction activation energy,  
46  
47 electron-ion carrier diffusion, and charge transfer across the internal resistance in the positive electrode, thus restricting the  
48  
49 battery's performance at low temperatures [36]. Taking the common lithium cobalt oxide (LiCoO<sub>2</sub>) cathode material as an  
50  
51 example, limited by the dynamics of the cathode material itself, the energy density of the ordinary commercial 18650 LiCoO<sub>2</sub>  
52  
53 battery at -40 °C is only 5% at room temperature [37]. Due to the above problems, the researchers made a series of targeted  
54  
55 modifications to the positive electrode to reduce the positive electrode material's influence on the battery's low-temperature  
56  
57  
58  
59  
60  
61  
62  
63  
64  
65

performance.

1  
2 Coating modifications on the surface of the cathode material are an effective means to improve the electron transport  
3  
4 characteristics of the cathode. The  $\text{LiNi}_{1/3}\text{Co}_{1/3}\text{Mn}_{1/3}\text{O}_2$  (NCM111) is coated with a layer of glassy  $\text{Li}_2\text{O}-2\text{B}_2\text{O}_3$  material to a  
5  
6 thickness of 8 nm to improve the capacity of the cathode material at  $-40\text{ }^\circ\text{C}$  [38]. When the cyclic performance test is carried  
7  
8 out at 0.2 C at  $-40\text{ }^\circ\text{C}$ , the specific capacity of the coated cathode is 3 times that of the initial sample ( $38\text{--}108\text{ mAhg}^{-1}$ ) [39].  
9  
10 Also, a similar improvement effect is confirmed in layered lithium-rich materials [40]. When  $\text{Li}_{1.2}\text{Ni}_{0.2}\text{Mn}_{0.6}\text{O}_2$  is deposited  
11  
12 in a layer of  $\text{Li}_3\text{BO}_3$  with a thickness of 5–6 nm on the surface of the lithium-rich material, a faster lithium-ion transmission  
13  
14 rate is obtained, and the cathode material can cycle stably at  $-30\text{ }^\circ\text{C}$  [41]. Furthermore, element doping is also an effective  
15  
16 way to improve the low-temperature discharge characteristics of cathode materials [42]. Doping a certain amount on the  
17  
18 surface of lithium-ion manganese oxide (LMO) batteries can effectively reduce the charge transfer potential of the material  
19  
20 and promote interfacial ion transport, improving the specific capacity of LMO at low temperatures.  
21  
22  
23  
24  
25  
26  
27  
28

29 The negative electrode's dynamic hysteresis of graphite material and the increase in interface impedance are the keys to  
30  
31 restricting the low-temperature performance of lithium-ion batteries. From the perspective of electrochemistry, the internal  
32  
33 resistance increase of charge transfer in the low-temperature conditions of the negative electrode is the core problem of  
34  
35 limiting the reaction and lithium-ion transfer [43]. The performance of the SEI film on the negative surface also has a  
36  
37 significant impact on the low-temperature battery performance. Therefore, most of the research on the improvement of low-  
38  
39 temperature negative electrode performance focuses on the above two aspects [44-46]. The pre-lithiation is introduced to  
40  
41 improve the specific discharge capacity of the graphite negative electrodes at low temperatures [47]. Due to the reduction of  
42  
43 internal resistance during charge transfer at low temperature, the pre-lithiation negative electrode material still has 67%  
44  
45 capacity retention at  $-40\text{ }^\circ\text{C}$ , which is far better than the untreated negative electrode material.  
46  
47  
48  
49  
50  
51  
52  
53

54 A self-supporting 3D graphene is prepared as the negative electrode material to improve the electrochemical performance  
55  
56 of the material at low temperatures by increasing electrochemical reaction sites and broadening lithium-ion transfer channels.  
57  
58 In combination with the electrochemical test and DFT calculation, the charge storage mechanism of this negative electrode  
59  
60  
61  
62  
63  
64  
65

1  
2 material, which depends on surface oxygen functional groups and defect sites, provides full play to the negative-material  
3 performance at low temperatures. Even after 100 cycles at -40 °C, the negative electrode material still has an actual specific  
4 capacity of 154 mAhg<sup>-1</sup> [48]. A new method is constructed to improve the low-temperature performance by reducing the  
5 internal resistance of the negative interface. The composition of the SEI between the positive and negative electrodes is  
6 adjusted at the same time to obtain an interface with a higher lithium-ion passing rate [49]. On the other hand, since the SEI  
7 containing decomposition products is more stable, it inhibits the further decomposition of electrolytes, which is conducive to  
8 controlling the thickness.  
9

10  
11 Many factors restrict the low-temperature performance of lithium-ion batteries, including both positive and negative  
12 electrodes, which are also inseparable from the electrolyte. Even though single-point modification can improve the low-  
13 temperature battery performance to a certain extent and meet the needs of specific environments [50]. However, for aviation-  
14 grade batteries, single-point modification is not enough. The operating conditions of these application scenarios are more  
15 stringent and require higher low-temperature battery performance [51]. In some conditions, it is required that the battery  
16 discharge current rate be 1 C at a cold temperature of -55 °C, and its capacity attenuation should not exceed 20% at room  
17 temperature. For the extreme usage requirements in aviation and other special fields, a set of overall collaborative  
18 optimization strategies has been established suitable for low-temperature lithium-ion batteries. It provides a significant  
19 scientific basis for the research and development of extremely low-temperature lithium-ion batteries.  
20  
21

22  
23 The dynamic characteristics of lithium-ion batteries lead to the difficulty of cycle life estimation, including high  
24 nonlinearity, robust time variability, and significant differences[52, 53]. It makes algorithm design with adaptive ability  
25 become a research hotspot. Time-series methods have achieved remarkable results, including H-infinity, support vector  
26 regression (SVR), Wiener process, and particle filter, among others, for accurate residual capacity estimation [54-56]. Data-  
27 driven enhancement of features has effectively realized model parameter correction purposes, including adaptive optimization  
28 and Gaussian process regression models [57-59]. With the rapid development of artificial intelligence methods, integration  
29 models and data-driven algorithms have made significant breakthroughs. It can simplify the evaluation process of complex  
30  
31

1 electrochemical battery reactions effectively [22, 60-63]. Deep learning (DL) methods can effectively improve the energy  
2 efficiency and reliability of the battery system to estimate the remaining cycle life value with robustness.  
3

4 The DL-based methods can effectively reflect the degradation trend of battery performance, including the long short-term  
5 memory (LSTM) and recurrent neural network (RNN) [64-66]. The efficient residual capacity estimation is realized by the  
6 mechanism analysis by combining LSTM and Elman neural networks, in which a mechanism analysis combining LSTM and  
7 Elman neural networks is realized by the mechanism analysis. These methods have the advantages of fast learning speed and  
8 good generalization performance [67-69]. By constructing the data-driven aging model, the Gaussian process regression and  
9 the LSTM are combined effectively [70]. Then, the residual capacity value is accurately estimated during the charging process  
10 based on voltage variation, current variation, and capacity reduction.  
11  
12  
13  
14  
15  
16  
17  
18  
19  
20  
21  
22

23 For the high-accuracy residual capacity estimation problems and deficiencies, combining with the development needs of  
24 extremely low operating temperatures for lithium-ion batteries in aerospace and other fields. The research procedure begins  
25 with the impact mechanism of energy attenuation and composite modeling theory. The model parameter changes are  
26 correlated with the battery performance to realize the multi-time scale evaluation at low temperatures, improving the carrier  
27 transport characteristics and speeding up the large-scale application of low-temperature lithium-ion batteries. The low-  
28 temperature performance is analyzed for the attenuation mechanism of lithium-ion batteries. The collaborative optimization  
29 mechanism is obtained for the composite modeling and carrier transport. Then, the robust multi-time-scale singular filtering-  
30 Gaussian process regression-long short-term memory (SF-GPR-LSTM) network through the coupling of multiple factors is  
31 constructed. It obtains the external performance and internal mechanism of low-temperature aging under the coupling  
32 relationship of multiple variables. A robust multi-state parameter synchronous estimation model is constructed to jointly  
33 optimize the transport process of carriers in a multi-component system, realizing battery performance optimization.  
34  
35  
36  
37  
38  
39  
40  
41  
42  
43  
44  
45  
46  
47  
48  
49  
50  
51  
52

## 53 2. Mathematical analysis 54 55

56 The information screening method of important influencing factors and collaborative estimation strategies of battery state  
57  
58  
59  
60  
61  
62  
63  
64  
65

parameters are analyzed for the residual capacity estimation when combined with the established composite battery model.

The multi-time-scale state parameter estimation optimized objective function is established. The robustness of short-time scale state parameter estimation is then enhanced through iterative calculation with adaptive capability. The correction algorithm is designed to form the improvement strategy of the SF-GPR-LSTM model with robustness to accurately estimate the multi-time scale state parameters through data fusion and correction under the influence of noise with nonlinear current variations.

### 2.1. State information screening and cooperative estimation strategy with noise impact correction

Consequently, the training set is optimized continuously, and the information screening methods are explored for key parameters using collaborative estimation strategies. Through the online model parameter correction, the mechanism of battery characteristics is described under different working conditions. The functional relationship between various parameters is obtained to realize the indirect mapping between the state-space equation and the state parameters for studying the linearization processing method of nonlinear dynamic characteristics. Combined with the key parameters and weighting factors, the feedback correction is realized by real-time calibration. The sliding time window function is used for filtering in the estimation process to recursively correct and improve the estimation accuracy of the constructed estimation model.

The theoretical analysis is carried out on the influencing factors of charge-discharge current, temperature, self-discharge rate, and aging effects by considering time variability and the complexity of application conditions. The influencing laws of key parameters are obtained in the iterative calculation process with mathematical characterization. Then, the functional relationship is obtained between model parameters and approximately linear current magnification. The structure for performance evaluation is designed for the modeling theory based on the correction of temperature and current magnification.

A closed-loop observer is constructed for the probability density function and the improvement strategy of the SF-GPR-LSTM model with robustness. A random vector dynamics model is set up to realize the approximate Gaussian distribution with a fixed number of sampling points, improving the adaptability of the estimation model to the dynamic working conditions.

The influence mechanism of multi-dimensional parameter constraints, such as working voltage, output current, and ambient temperature, is clarified, integrating a variety of environmental impact factors into the iteration in combination with the multivariate parameter estimation theory. The impact of the estimation process is analyzed to determine the weight coefficient in combination with the observed value and prior distribution information. Then, the new data point set is calculated and applied to improve the real-time adaptability of the model, realizing the optimization process by integrating the weighting operation. Three gate structures are introduced with different control functions, namely the forget gate, input gate, and output gate. These gate structures are built to learn some useful long-term information and discard some unnecessary information, so as to play the function of information screening. The framework is constructed for the long-timescale residual capacity estimation model, as shown in Figure 1.

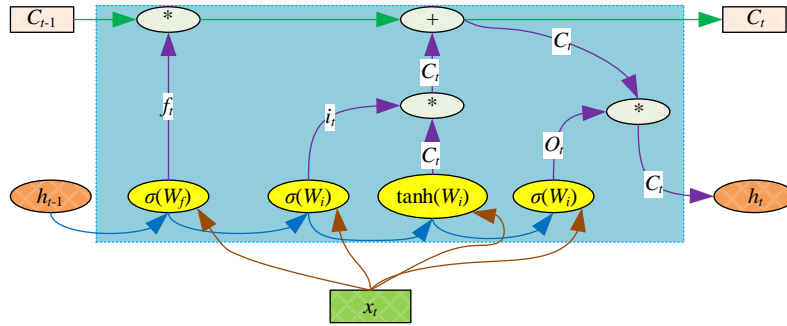


Figure 1. Multi-time scale residual capacity estimation based on the LSTM deep learning strategies

In Figure 1,  $x_t$  is the input data sequence, which is the system condition monitoring information used for fault estimation.  $h_t$  is the hidden state or the learning output of each LSTM unit.  $f_t$  is the forget gate.  $i_t$  is the input gate.  $O_t$  is the output gate,  $\sigma$  is the sigmoid activate function, and  $\tanh(\cdot)$  is the hyperbolic tangent function.  $W$  and  $b$  are the weight matrix and bias vectors attached to each gate and  $*$  is the Hadamard multiplication product.

The forget gate processes time series data in a specified order in the LSTM network, determining what information to retain for a given period and what information to ignore outright. The mathematical expression of the forget gate is designed, as shown in Equation (1).

$$f_t = \sigma * (W_f[h_{t-1}, x_t] + b_f) \quad (1)$$

In Equation (1),  $W_f$  is the weight and  $b_f$  is the bias vector attached to the forget gate. Then, the current input information enters the input gate, and the previous hidden state  $h_{t-1}$  and passes them through the  $\sigma$  and  $\tanh$  layers. The function of the input gate is to judge which parameters need to be updated and how to update them. The mathematical expression of the input gate and the cell is designed, as shown in Equation (2).

$$\begin{cases} i_t = \sigma * (W_i[h_{t-1}, x_t] + b_i) \\ \tilde{C}_t = \tanh * (W_C[h_{t-1}, x_t] + b_C) \\ C_t = f_t * C_{t-1} + i_t * \tilde{C}_t \end{cases} \quad (2)$$

In Equation (2),  $W_i$  and  $W_C$  are the corresponding weight coefficient and  $b_i$  and  $b_C$  are the corresponding bias vectors attached to the input gate and the cell state, respectively.  $C_t$  is the cell state information at time point  $t$ .

The output gate functions after the information have been filtered by the forget gate and the input gate. The function of the output gate is to decide which information to output. The mathematical expression of the output gate is designed, as shown in Equation (3).

$$\begin{cases} O_t = \sigma * (W_o[h_{t-1}, x_t] + b_o) \\ h_t = O_t * \tanh(C_t) \end{cases} \quad (3)$$

In Equation (3),  $W_o$  and  $b_o$  are the weight and the bias vector attached to the output gate, respectively.  $h_t$  is the output value of the present unit.

The advantage of LSTM is that it can refer to information from previous cells when processing information from this cell, but it cannot process information from cell to cell. Some problems are related not only to the previous unit information but also to the subsequent unit information, such as the state parameters that reflect the system's performance degradation process. Due to the inaccurate observation or data uncertainty in the sensor acquisition process, the parameters collected at the previous and subsequent times confirm the accuracy of the current time parameters. Therefore, the SF-GPR-LSTM model can learn the laws of forwarding and backward information simultaneously.

The performance attenuation mechanism and life estimation procedure are designed by considering aging inducements such as different temperatures, current magnification, and interactive stress effects. The model parameters are modified through recursive calculation and output feedback by combining the time and state updates. The model parameters in the

state-space equation are optimized synchronously by feedback to improve the estimation accuracy. Also, the model structure is optimized to improve the adaptability of complex working conditions for the residual capacity to verify and optimize the accuracy and robustness of the estimation model.

## 2.2. Dual closed-loop observer for the short-time scale multi-state parameter cooperative estimation

A deep learning-based information fusion theory is introduced to carry out multi-task training and optimization with a highly adaptive extreme low-temperature multi-state parameter estimation model. The state estimation robustness is improved through iterative calculation. The dynamic characteristics of ambient temperature, battery aging, and current magnification are fully considered. The pre-trained network is obtained through the transfer learning mechanism to reduce the burden of the model on learning tasks. It learns not only the information from the previous time step but also that of the future. It solves the problem of one-way time-sequence calculation and improves the weighting matrix, which is greatly affected by time sequence. The functional relationship between the parameters is proved through the neural layer structure fine-tuning exploration, and the mathematical mapping between state equation and battery performance is realized. The dual closed-loop observer framework based on deep learning is constructed, as shown in Figure 2.

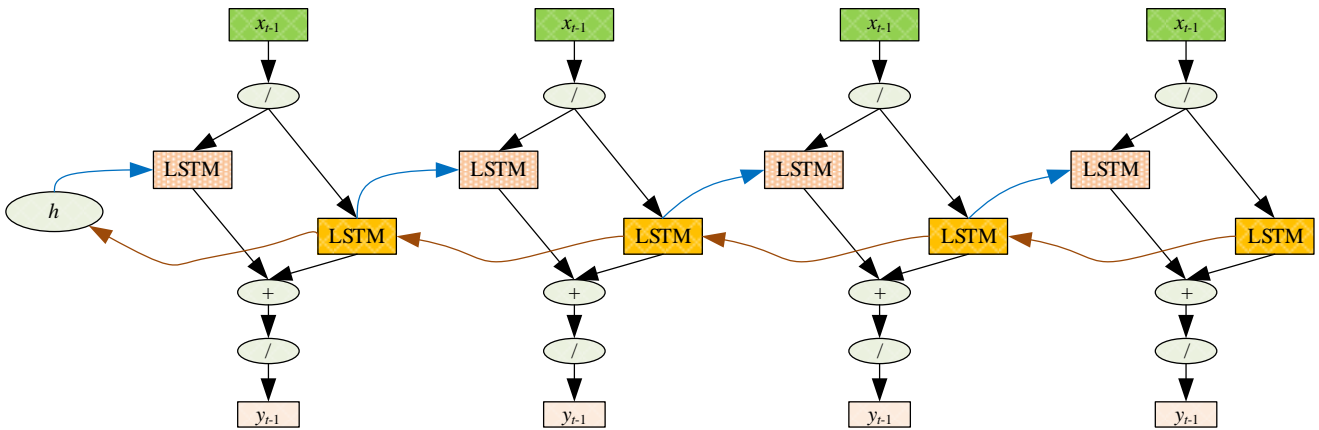


Figure 2. LSTM-based cooperative estimation framework for short-term scale multi-state parameters

In Figure 2, the adaptive correction method of characteristic information is studied by considering the noise interference factors in externally measurable parameters. The strategy of model parameter improvement and weight factor correction is

explored by improving the weight calculation process and superimposing the aging coefficient. A systematic battery sample test set is established with the impact of different initial conditions. The hidden layer stores the vector  $\vec{h}$  obtained by the forwarding estimation and the vector  $\bar{h}$  obtained by reverse inference, and its calculation is based on one-way LSTM. Then, the final output result  $y_t$  is formed by the combination of  $\vec{h}$  and  $\bar{h}$ , as shown in Equation (4).

$$\begin{cases} \vec{h} = \text{LSTM}(x_t, \vec{h}_{t-1}) \\ \bar{h}_t = \text{LSTM}(x_t, \bar{h}_{t+1}) \\ y_t = g(W_{\vec{h}y}\vec{h}_t + W_{\bar{h}y}\bar{h}_t + b_y) \end{cases} \quad (4)$$

In Equation (4), the differences between various working modes are characterized efficiently to improve the accuracy of multi-state parameter estimation. The coupling mechanism is clarified by taking the obtained detection and filtering results of external battery parameters as the input of the network, based on multi-objective state estimation theory and a cooperative state estimation method. Then, the filtered matrix is taken as the intermediate state parameter, and each state parameter is input into the other. An iterative calculation is obtained with strong adaptability, and the multi-state parameter collaborative estimation model with strong anti-noise ability is effectively constructed.

### 2.3. Feedback modification of model parameters and cooperative optimization of carrier transports

The influence factors of environmental variables and the aging effect are considered, and the adaptive adjustment mechanism is added based on the characteristic model. The double unscented transformation closed-loop observer is constructed by considering the probability density function to judge the effectiveness of the optimization strategy for the cathode, anode, electrolyte, and SEI layer at low temperatures of lithium-ion batteries. The weight coefficient is distributed based on the observed and prior state values. The time and state parameters are updated through recursive calculation and correction. A variety of characteristics are integrated with adaptive correction. A multi-level performance evaluation system is constructed to improve the adaptability of the method. It helps in achieving an accurate mathematical description of the state-space modeling parameters to guide the collaborative optimization and improvement of the physical carrier transport properties.

The state-space equation is constructed for the model parameters and adaptive weight coefficients to the present

1  
2 distribution. The process model is established to reflect the characteristics of the working condition by considering the  
3 influence of the current ratio and temperature. The preset and distribution are realized for both model parameters and weight  
4 coefficients. Under multiple constraints, a model parameter estimation strategy based on temperature correction is constructed.  
5  
6 Higher model expression accuracy is obtained by analyzing the multiple parameter constraints. It greatly reduces the  
7  
8 estimation error of model parameters caused by noise interference to realize a more accurate evaluation.  
9  
10

11  
12 The strategy comprehensively considers the influence of modeling and battery state parameters. The problem of  
13 environmental impact in the state estimation process is solved using the full parameter online identification model and  
14  
15 capacity-temperature correction, ensuring the accuracy and adaptability of battery state parameter calculation. The equivalent  
16  
17 parameters are transferred to the iterative calculation by the state-space equation to improve the adaptability of the model  
18  
19 based on the characteristic mathematical description of different working conditions. The output response variation law of  
20  
21 the estimation model is studied under different conditions. Then, the influence of the current fluctuation and temperature  
22  
23 change on the battery performance is considered with the model structure optimization. Then, the discrete nonlinear dynamic  
24  
25 system modeling structure is established, and the state variables are recursively calculated.  
26  
27  
28  
29  
30  
31

32  
33 Continuous improvement is conducted for carrier-transport cooperative optimization. Given the limited effect of single-  
34  
35 component optimization on the performance improvement of extremely low-temperature lithium-ion batteries, the  
36  
37 collaborative optimization mechanism is studied for multiple components and methods. The main influencing parameter  
38  
39 studied as the battery's internal resistance increases are the charge transfer resistance ( $R_{CT}$ ) and the SEI resistance ( $R_{SEI}$ ). The  
40  
41 speed-limiting steps of collaborative carrier transport are quickly deduced in multicomponent materials, such as solid ion  
42  
43 diffusion of inert materials, ion migration in the electrolyte, and charge transfer at the phase interface. The carrier transport  
44  
45 optimization strategy is realized based on the analysis results of the above composite battery model. Then, the optimization  
46  
47 strategy is verified by model iteration to realize the spiral rise of low-temperature battery performance. The iterative process  
48  
49 of battery material design and verification is reduced through the rapid analysis ability of the composite model. The rapid  
50  
51 optimization of active materials matching extremely low-temperature batteries is realized, as shown in Figure 3.  
52  
53  
54  
55  
56  
57  
58  
59  
60

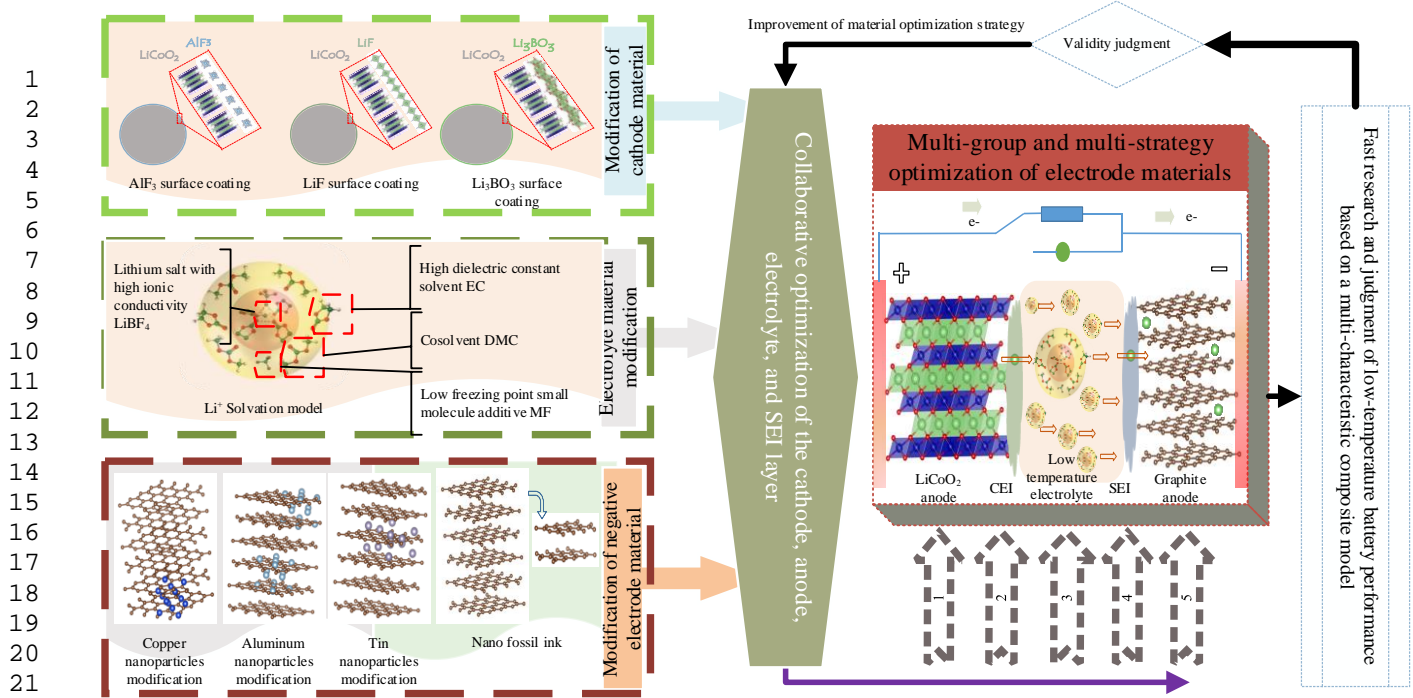


Figure 3. Continuous improvement of collaborative optimization for active battery materials

In Figure 3, multi-component and multi-strategy collaborative optimization for the low-temperature battery characteristics mainly starts with the modification of the physical intrinsic low-temperature dynamic characteristics. The low-temperature electrolyte must meet three basic requirements. First, the high dielectric constant (89.5% - 78@25 °C) is conducted to ensure lithium salt solubility. Then, EC is the preferred main solvent for low-temperature electrolytes, and DMC is an excellent cosolvent. It can further accelerate the migration speed of lithium-ions. Second, a lower viscosity or freezing point (less than -80 °C) ensures effective electrolyte and electrode particle infiltration. Among them, the freezing point of the small molecule additive methyl formate (MF) is below -99 °C, which makes it a better choice for low-viscosity, low-temperature electrolytes. Third, the matched lithium salt ensures high lithium-ion conductivity (greater than 1 mS/cm) at low temperatures. Lithium tetrafluoroborate (LiBF<sub>4</sub>) has proven to have better low-temperature capacity retention characteristics at -40 °C.

Lithium cobaltate's intrinsic insertion reaction dynamics (LiCoO<sub>2</sub>) have been enough to meet the Li<sup>+</sup> migration under low-temperature conditions. The low-temperature performance modification strategy focuses on the charge transfer process at the interface between cathode particles and electrolytes. The cathode SEI layer is the key to the surface of the particles. AlF<sub>3</sub> is an excellent lithium-ion conductor that promotes Li<sup>+</sup> transfer under low-temperature conditions. It is a potential

1  
2  
3  
4  
5  
6  
7  
8  
9  
10  
11  
12  
13  
14  
15  
16  
17  
18  
19  
20  
21  
22  
23  
24  
25  
26  
27  
28  
29  
30  
31  
32  
33  
34  
35  
36  
37  
38  
39  
40  
41  
42  
43  
44  
45  
46  
47  
48  
49  
50  
51  
52  
53  
54  
55  
56  
57  
58  
59  
60  
61  
62  
63  
64  
65

modification scheme for cathode materials. The anode material, cathode material, graphite, and SEI layer are the keys to the attenuation of low-temperature performance. From the perspective of the electrochemical process, inhibiting charge transfer resistance, SEI resistance, and ion diffusion resistance in graphite in a low-temperature environment are the main directions to improve the capacity and magnification characteristics.

The main source of charge transfer and SEI resistance is the solvation and desolvation processes of the lithium-ions. In particular, the desolvation process is the main energy-consuming step. The activation energy of the desolvation process on the graphite surface exceeds 60 kJ/mol, which is the main speed-limiting step with the temperature decrease. The addition of nano-metal tin (Sn) particles plays a similar role to the catalyst. It shows an excellent low-temperature performance improvement effect for reducing the energy barrier of desolvation. The reason for the increase in ion diffusion resistance of the graphite bulk phase is the non-equilibrium lithium process. More than three different phases are determined by neutron diffraction. The uniformity of lithium is effectively improved by reducing the size of graphite particles and improving the conductivity of lithium-ion batteries at low temperatures.

#### 2.4. Performance evaluation index factors

In the residual capacity estimation process, the RMSE, MSE, MAE, and R-squared metrics are employed for the critical evaluation of the performance of the proposed SF-GPR-LSTM model. The RMSE is calculated by the square root calculation of the evaluation ratio for the square of the deviation to the number of samples  $m$  to indicate the degree of dispersion. The deviation is obtained by the residual calculation between the actual value ( $y_i$ ) and the estimated value ( $\hat{y}_i$ ). The RMSE is used to measure the deviation between the observed value and the true value. The expression for the calculation of the RMSE is shown in Equation (5).

$$RMSE = \sqrt{\frac{1}{m} \sum_{i=1}^m (y_i - \hat{y}_i)^2} \quad (5)$$

The MSE is used to evaluate the expected square value of the difference between the estimated value and the true value of the residual capacity. The MSE is calculated by squaring the difference between the actual and estimated values and then

averaging the sum. The expression for the calculation of the MSE is shown in Equation (6).

$$MSE = \frac{1}{m} \sum_{i=1}^m (y_i - \hat{y}_i)^2 \quad (6)$$

The MAE is the average of absolute errors. It can better reflect how the estimated error value is individually weighted equally around the actual value (the positive and negative offset each other). The expression for the calculation of the MAE is shown in Equation (7).

$$MAE = \frac{1}{m} \sum_{i=1}^m |y_i - \hat{y}_i| \quad (7)$$

The R-squared (coefficient of determination) value is calculated based on the sum of squares of residuals (RSS) and the total sum of squares (TSS). The RSS is the sum of the squares of the difference between the actual value ( $y_i$ ) and the estimated data ( $\hat{y}_i$ ), and its calculation is shown in Equation (8).

$$RSS = \sum_{i=1}^m (y_i - \hat{y}_i)^2 \quad (8)$$

The TSS is the square sum of the difference between the actual value ( $y_i$ ) and the mean value ( $\bar{y}$ ). Its calculation is shown in Equation (9).

$$TSS = \sum_{i=1}^m (y_i - \bar{y})^2 \quad (9)$$

The R-squared represents the perfection of a fitting model in accurately estimating the residual capacity of the actual value. It is defined as the ratio of RSS and TSS. Its calculation is obtained, as shown in Equation (10).

$$\text{R-squared} = \frac{TSS - RSS}{TSS} = 1 - \frac{RSS}{TSS} \quad (10)$$

### 3. Experimental analysis

#### 3.1. Experimental platform design

Multi-level performance testing and evaluation are conducted to verify and improve the composite battery model. The effectiveness of composite modeling and collaborative carrier transport optimization methods is validated when combined with the embedded application of the method. The characteristic variations of open-circuit voltage and temperature capacity

are analyzed. The pulse response characteristics are the focus of the lithium-ion battery model construction and theoretical analysis. The characteristic experiments are designed and carried out for the lithium-ion battery to realize full sampling and quantitative analysis of experimental data under the influence of low temperatures using the established experimental platform and test process. The equipment includes the charge-discharge tester, a temperature chamber, and other supporting experimental equipment, providing appropriate environmental working conditions. The experimental platform and testing procedure are designed, as shown in Figure 4.

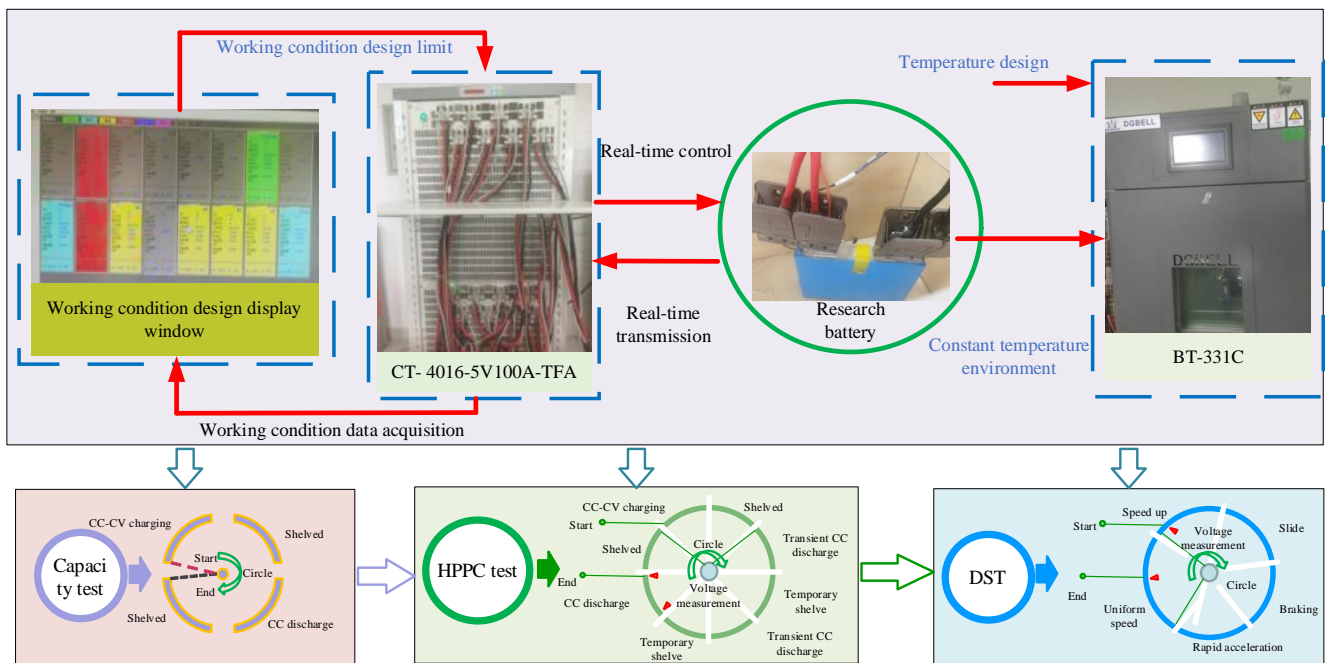


Figure 4. The experimental platform and the test procedure for multi-timescale performance of lithium-ion batteries

In Figure 4, the CT-4016-5V 100A-TFA is a charge-discharge tester, often used for battery cycle life tests, battery capacity tests, battery charging characteristic tests, battery discharge characteristic tests, battery charge retention ability tests, battery charging and discharging efficiency tests, battery overcharge, over-discharge rate endurance tests, etc. The BT-331C is a programmable thermostat, which is used to set the ambient temperature of the battery required for the experiment to achieve the experimental effect of extremely low temperature. The characteristic analysis of lithium-ion batteries is inseparable from the joint action of test methods and data. Based on the experimental process shown in the figure, the experiments on the characteristics of lithium-ion batteries are obtained at different temperatures (-60, -40, -20, 0, 30, and 60 °C). The

1  
2 experimental data of capacity test, hybrid power pulse characterization (HPPC) test and dynamic stress test (DST) under  
3 three working conditions are obtained. The input parameter detection accuracy is analyzed with the model parameters using  
4 different initial state quantity conditions. The experimental effect analysis under the influence of dynamic noise is carried out  
5  
6 to explore the dynamic relationship between lithium-ion battery performance and model output results. It is used to quickly  
7  
8 determine the carbon source and reaction temperature. The collaborative carrier transport optimization parameters are  
9  
10 improved recursively by combining them with the physical property process based on the reaction time and air pressure  
11  
12 influence on the battery's performance.  
13  
14  
15  
16

17  
18 Six cells are used for the aging test experiment to explore the aging characteristics of lithium-ion batteries. For the rapid  
19  
20 aging test, batteries #1, #2, and #3 are used for the remaining capacity estimation. Under the Beijing bus dynamic stress test  
21  
22 (BB DST) working condition, batteries #4, #5, and #6 are used for the aging test. The aging modeling of batteries is carried  
23  
24 out using the test results. The aging model is realized by the SF-GPR-LSTM model, which is constructed using MATLAB  
25  
26 R2019a, and the experimental result is plotted using Origin 2018 software.  
27  
28  
29  
30  
31

### 32 *3.2. Capacity decay and aging estimation effect analysis*

33  
34

35 The capacity value obtained during the battery operation is susceptible to various uncertainties, so the collected data  
36  
37 contains a lot of noise and fluctuation. If the original data is directly used for modeling without data preprocessing, the model  
38  
39 accuracy will be greatly reduced. The necessary data preprocessing process helps to improve the estimation accuracy of the  
40  
41 model. Through the proposed adaptive data preprocessing, the original capacity data is smoothed and denoised so that the  
42  
43 processed data has a monotonic downward trend to learn the degradation trend in early life. The residual capacity estimation  
44  
45 is carried out to obtain more accurate results using the established SF-GPR-LSTM model. The estimation effects are analyzed  
46  
47 under different conditions to test the adaptive ability of different training lengths. The estimation effect has the same adaptive  
48  
49 ability and degradation trend as the original data set through the verification of a highly robust effect at different starting time  
50  
51 points. The model training process is shown in Figure 5.  
52  
53  
54  
55  
56  
57  
58  
59  
60  
61  
62  
63  
64  
65

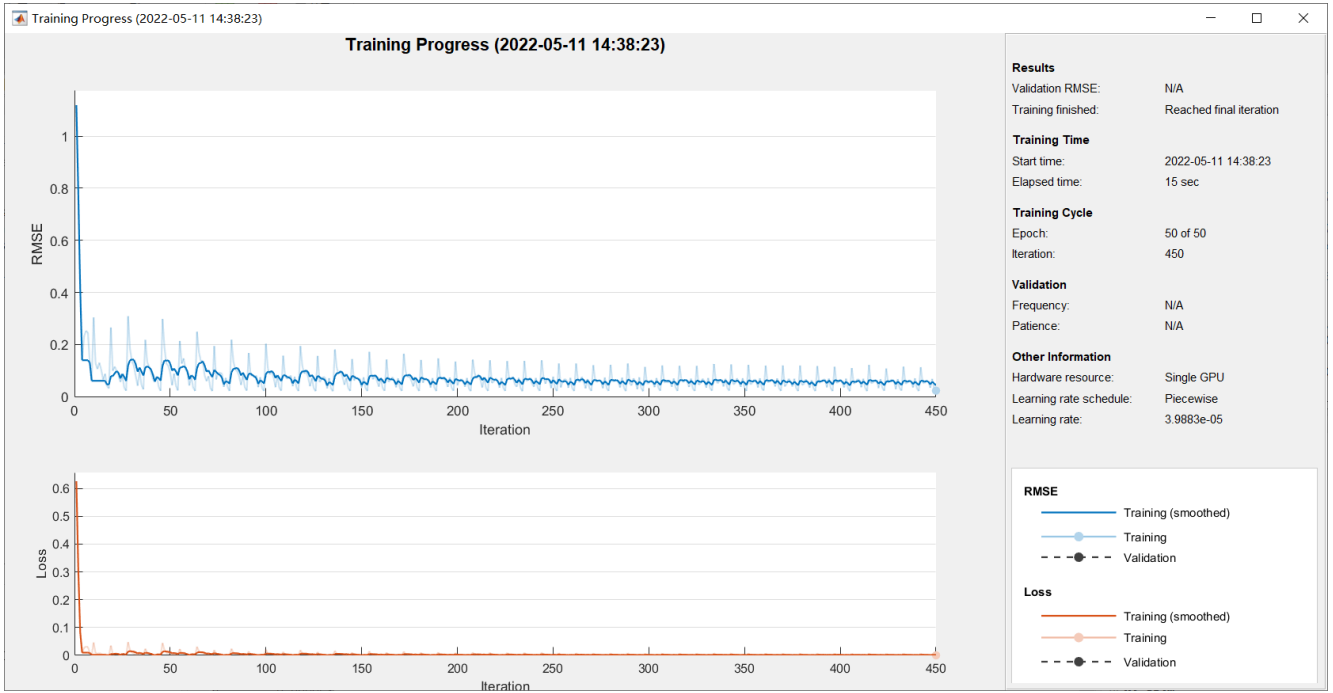
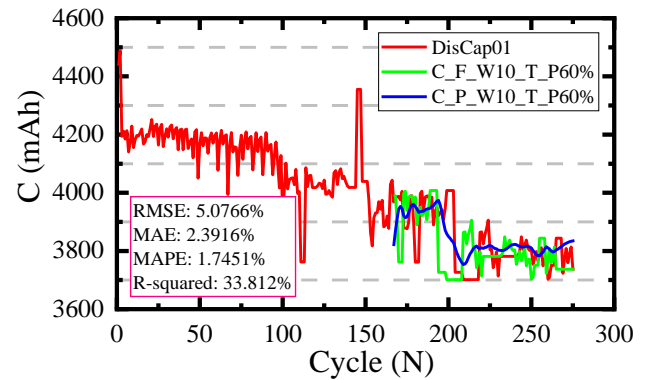
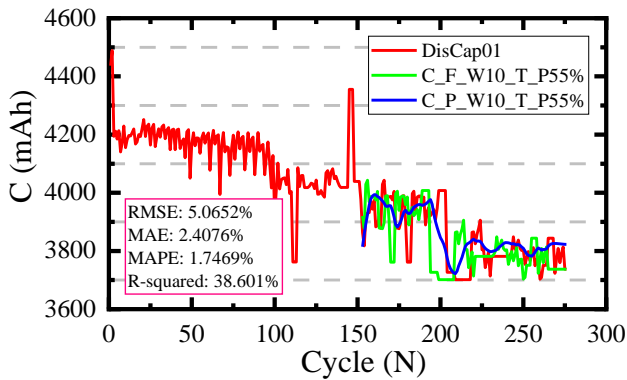


Figure 5. The training progress interface of the SF-GPR-LSTM neural network

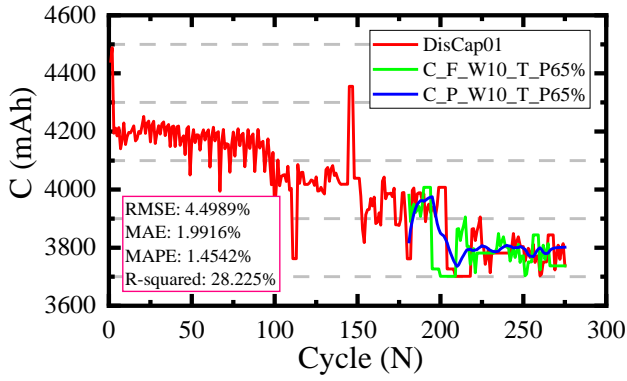
In Figure 5, the residual capacity training effect of the proposed method is verified using whole-life-cycle experimental test data using battery #2 for verification. The recorded capacity dataset is used for the training and testing processes. The whole-life-cycle change adaptability considers the cycle test data, in which the discharge capacity is analyzed as the main change component. In model effect analysis, the experimental discharge capacity data is divided into two parts: the first is used for training, and the latter is used for testing or estimation. The input proportions of the testing datasets are 55%, 60%, 65%, and 70%. The estimation results are obtained at  $-20^{\circ}\text{C}$  for the original experimental data, filtered data for estimation, and estimation results for battery #1, respectively, as shown in Figure 6.



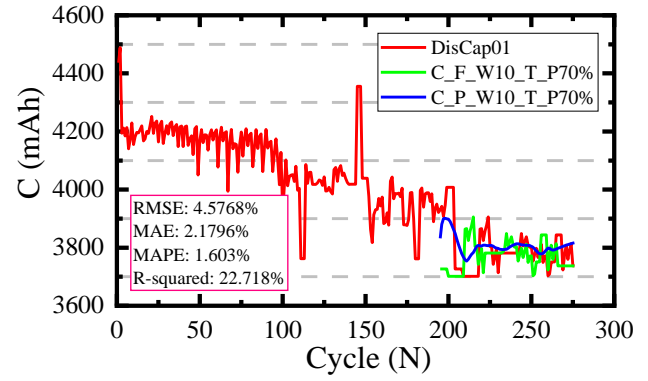
(a) Estimating the remaining capacity variation with W10\_

(b) Estimating the remaining capacity variation with W10\_

T\_ P55% dataset



T\_ P60% dataset



(c) Estimating the remaining capacity variation with W10\_

(d) Estimating the remaining capacity variation with W10\_

T\_ P65% dataset

T\_ P70% dataset

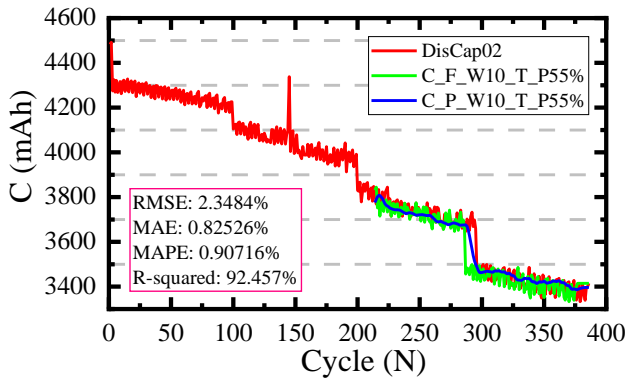
Figure 6. Capacity estimation adapting to different training test datasets during rapid aging (battery #1)

In Figure 6, W10 is the filtering window with a width of 10, This value have a better estimation effect compared with other window width values. The model's adaptability is verified based on the different proportions of the training sample set and estimation sample set. Then, the estimation effect is evaluated using RMSE, MAE, MAPE, and R-squared result evaluation metrics. It can be seen that the higher the proportion, proportion the better the adaptability of the model and the higher the estimation accuracy. Even when using 55% of the datasets to estimate the remaining capacity, the estimation effect is good for an RMSE value of 5.0652%, an MAE value of 2.4076%, and a MAPE value of 1.7469%, together with the R-squared value of 38.601% using 55% of the dataset. The results for the various proportions of datasets used are presented to verify the estimation effect for the improved SF-GPR-LSTM model, which is adaptive to the fast-charging complex current variation conditions.

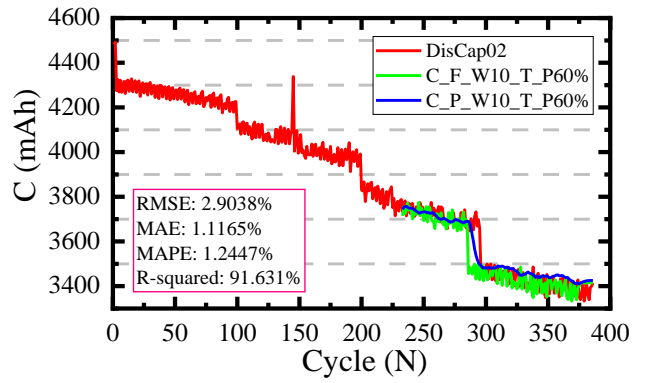
### 3.3. Strong volatility adaptability analysis

The capacity data of battery #2 is selected for effect analysis, filled with large fluctuations in discharge capacity measurement and unstable performance to analyze the adaptability of the constructed model. The discharge capacity data fluctuates violently in the later stages. In the analysis process, considering the singularity of capacity variations in the original data, the singular data is filtered and preprocessed. The reasonable variation in the normal capacity between adjacent cycles

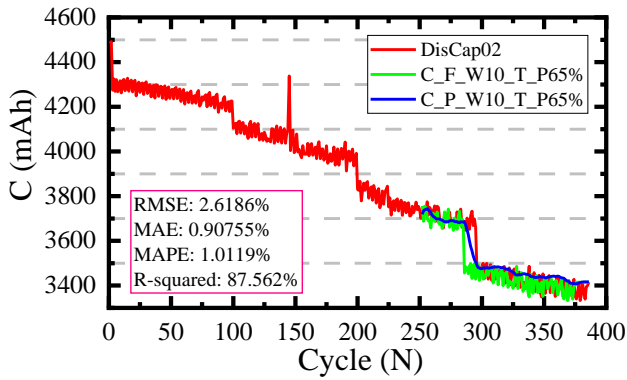
is no more than 10%. The estimated results at  $-40^{\circ}\text{C}$  are shown in Figure 7.



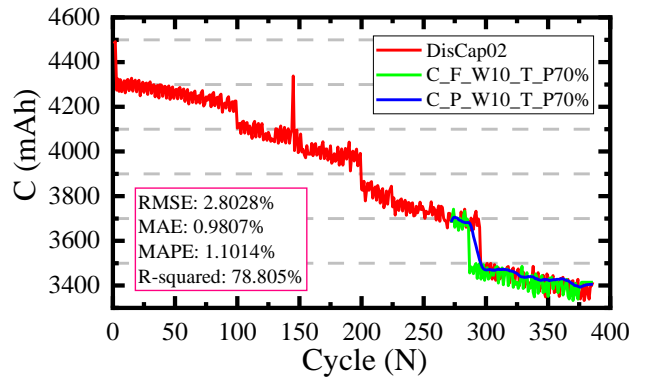
(a) Estimating the remaining capacity variation with W10\_  
T\_P55% dataset



(b) Estimating the remaining capacity variation with W10\_  
T\_P60% dataset



(c) Estimating the remaining capacity variation with W10\_  
T\_P65% dataset



(d) Estimating the remaining capacity variation with W10\_  
T\_P70% dataset

Figure 7. Capacity estimation adaptive to different training test datasets during rapid aging (battery #2)

In Figure 7, the estimation results are provided for four different dataset sizes. It can be observed from the experimental results that the estimation effect is good under different conditions. The improved SF-GPR-LSTM model estimates the remaining capacity using 55% of the data set with an RMSE value of 2.3484%, an MAE value of 0.82526%, a MAPE value of 0.90716%, and an R-squared value of 92.457%. Its degradation trend is similar to the attenuation trend of the original capacity. Experimental results show that this model has high estimation accuracy and robustness under extreme low temperature conditions, laying a theoretical foundation for the whole-life-cycle battery remaining capacity estimation at extremely low temperatures.

### 3.4 Critical verification of the proposed method

Finally, the graphical representation of the proposed model's RMSE, MAE, MAPE, and R-squared values in Figures 6 and 7 are plotted using different testing datasets for batteries #1 and #2, as shown in Figure 8.

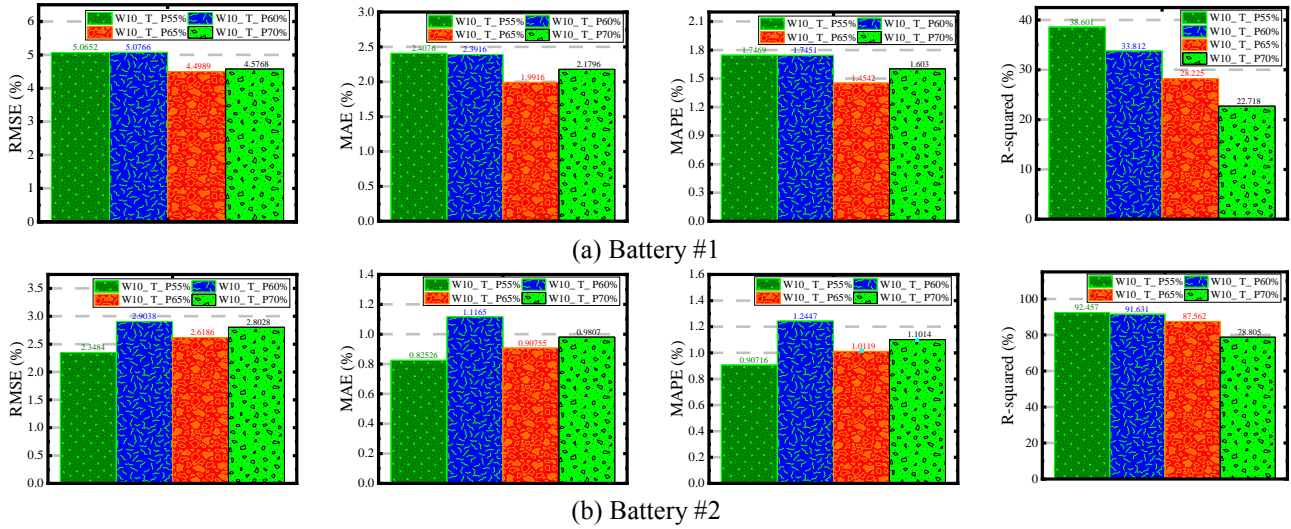


Figure 8. Verification results of the proposed SF-GPR-LSTM model

When the values of the various metrics are compared in Figure 8, it is clear that, with a sliding window size of 10 and different sizes of testing datasets. RMSE, MAE and MAPE are within 5.0652%, 2.4076% and 1.7469%, respectively, and R can be as high as 92.457%. These values are highly optimal for real-time capacity estimation at different training and estimation cycles for lithium-ion batteries.

### 4. Conclusion

For efficient and accurate remaining capacity estimation, which is of great significance to study the adaptability of lithium-ion batteries under extreme low temperature. An improved SF-GPR-LSTM model is constructed by considering multi-time scale factors to overcome the difficulty of accurate remaining capacity estimation. The recursive calculation and data distribution models are optimized. Then, a deep learning network is constructed by balancing computational cost and accuracy. A strong adaptive estimation algorithm is constructed that is combined with iterative optimization. For battery #1, using 55% of the datasets, the estimation of the remaining capacity has an RMSE value of 5.0652%, an MAE value of 2.4076%, a MAPE value of 1.7469%, and an R-squared value of 38.601% using 55% of the dataset. For battery #2, using 55% of the dataset, an RMSE value of 2.3484%, an MAE value of 0.82526%, a MAPE value of 0.90716%, and an R-squared value of 92.457%.

1  
2  
3  
4  
5  
6  
7  
8  
9  
10  
11  
12  
13  
14  
15  
16  
17  
18  
19  
20  
21  
22  
23  
24  
25  
26  
27  
28  
29  
30  
31  
32  
33  
34  
35  
36  
37  
38  
39  
40  
41  
42  
43  
44  
45  
46  
47  
48  
49  
50  
51  
52  
53  
54  
55  
56  
57  
58  
59  
60  
61  
62  
63  
64  
65

Meanwhile, all the other error values for both batteries show that the SF-GPR-LSTM model has high residual capacity estimation accuracy with small estimation errors and good stability, which provides a reference for the residual capacity estimation of lithium-ion batteries. The proposed SF-GPR-LSTM estimation method has a characteristic theory that reveals the modeling mechanism and optimization mechanism. By deeply analyzing the battery characteristics, the co-carrier optimization of lithium ion and electron transport is carried out, and a robust cycle life estimation model suitable for complex working conditions is established, laying the theoretical foundation for the industrial application of lithium-ion batteries.

## Acknowledgment

The work is supported by the National Natural Science Foundation of China (No. 62173281), the Natural Science Foundation of Sichuan Province (No. 23ZDYF0734, 2023NSFSC1436), and the Fund of Robot Technology used for Special Environment Key Laboratory of Sichuan Province (No. 18kftk03).

## References

1. Zhang, Q., et al., *A deep learning method for lithium-ion battery remaining useful life prediction based on sparse segment data via cloud computing system*. Energy, 2022. **241**: p. 1-11.
2. Zhang, M., et al., *A method for capacity prediction of lithium-ion batteries under small sample conditions*. Energy, 2022. **238**: p. 1-12.
3. Ye, Z. and J. Yu, *State-of-Health Estimation for Lithium-Ion Batteries Using Domain Adversarial Transfer Learning*. IEEE Transactions on Power Electronics, 2022. **37**(3): p. 3528-3543.
4. Wang, W., L.W. Fan, and P. Zhou, *Evolution of global fossil fuel trade dependencies*. Energy, 2022. **238**: p. 1-12.
5. Tang, T. and H. Yuan, *A hybrid approach based on decomposition algorithm and neural network for remaining useful life prediction of lithium-ion battery*. Reliability Engineering & System Safety, 2022. **217**: p. 1-13.
6. Pan, D., H. Li, and S. Wang, *Transfer Learning-Based Hybrid Remaining Useful Life Prediction for Lithium-Ion Batteries Under Different Stresses*. IEEE Transactions on Instrumentation and Measurement, 2022. **71**: p. 1-22.
7. Hu, J., et al., *Disturbance-Immune and Aging-Robust Internal Short Circuit Diagnostic for Lithium-Ion Battery*. IEEE Transactions on Industrial Electronics, 2022. **69**(2): p. 1988-1999.
8. Greenbank, S. and D. Howey, *Automated Feature Extraction and Selection for Data-Driven Models of Rapid Battery Capacity Fade and End of Life*. IEEE Transactions on Industrial Informatics, 2022. **18**(5): p. 2965-2973.
9. Ge, Y., F. Zhang, and Y. Ren, *Lithium Ion Battery Health Prediction via Variable Mode Decomposition and Deep Learning Network With Self-Attention Mechanism*. Frontiers in Energy Research, 2022. **10**: p. 1-15.
10. Chen, Z., et al., *Remaining Useful Life Prediction of Lithium-Ion Battery via a Sequence Decomposition and Deep Learning Integrated Approach*. IEEE Transactions on Vehicular Technology, 2022. **71**(2): p. 1466-1479.
11. Zuo, J., et al., *Deep learning based prognostic framework towards proton exchange membrane fuel cell for automotive application*. Applied Energy, 2021. **281**: p. 1-13.
12. Zraibi, B., et al., *Remaining Useful Life Assessment for Lithium-Ion Batteries Using CNN-LSTM-DNN Hybrid Method*. IEEE Transactions on Vehicular Technology, 2021. **70**(5): p. 4252-4261.
13. Zou, H., et al., *Stochastic multi-carrier energy management in the smart islands using reinforcement learning and unscented transform*. International Journal of Electrical Power & Energy Systems, 2021. **130**(106988): p. 1-12.

14. Zhuang, P. and H. Liang, *False Data Injection Attacks Against State-of-Charge Estimation of Battery Energy Storage Systems in Smart Distribution Networks*. IEEE Transactions on Smart Grid, 2021. **12**(3): p. 2566-2577.
15. Zhu, J.G., et al., *Investigation of capacity fade for 18650-type lithium-ion batteries cycled in different state of charge (SoC) ranges*. Journal of Power Sources, 2021. **489**(7): p. 1-12.
16. Zhou, S.D., et al., *Adaptive model parameter identification for lithium-ion batteries based on improved coupling hybrid adaptive particle swarm optimization- simulated annealing method*. Journal of Power Sources, 2021. **482**: p. 1-12.
17. Zhou, L., M. Parhizi, and A. Jain, *Theoretical analysis of transient solution phase concentration field in a porous composite electrode with time-dependent flux boundary condition*. Journal of Applied Electrochemistry, 2021. **51**(9): p. 1241-1252.
18. Zhengxin, J., et al., *An Immune Genetic Extended Kalman Particle Filter approach on state of charge estimation for lithium-ion battery*. Energy, 2021. **230**(52): p. 1-14.
19. Zheng, Y.J., et al., *A simplification of the time-domain equivalent circuit model for lithium-ion batteries based on low-frequency electrochemical impedance spectra*. Journal of Power Sources, 2021. **489**: p. 1-12.
20. Yu, L., et al., *Boosting lithium batteries under harsh operating conditions by a resilient ionogel with liquid-like ionic conductivity*. Journal Of Energy Chemistry, 2021. **62**: p. 408-414.
21. Zhao, X.H., et al., *Sulfurized polyacrylonitrile for high-performance lithium sulfur batteries: advances and prospects*. Journal Of Materials Chemistry A, 2021. **9**(35): p. 19282-19297.
22. Zhao, M.H., et al., *Deep Residual Networks With Adaptively Parametric Rectifier Linear Units for Fault Diagnosis*. IEEE Transactions on Industrial Electronics, 2021. **68**(3): p. 2587-2597.
23. Zhang, T., et al., *A Systematic Framework for State of Charge, State of Health and State of Power Co-Estimation of Lithium-Ion Battery in Electric Vehicles*. Sustainability, 2021. **13**(9): p. 1-19.
24. Zhang, S.Z., X. Guo, and X.W. Zhang, *A novel one-way transmitted co-estimation framework for capacity and state-of-charge of lithium-ion battery based on double adaptive extended Kalman filters*. Journal of Energy Storage, 2021. **33**(1): p. 1-16.
25. Xu, W.H., et al., *A novel adaptive dual extended Kalman filtering algorithm for the Li-ion battery state of charge and state of health co-estimation*. International Journal of Energy Research, 2021. **45**(12): p. 14592-14602.
26. Xu, T., Z. Peng, and L. Wu, *A novel data-driven method for predicting the circulating capacity of lithium-ion battery under random variable current*. Energy, 2021. **218**(119530): p. 1-13.
27. Vasilyev, A., et al., *Dynamic Reliability Assessment of PEM Fuel Cell Systems*. Reliability Engineering & System Safety, 2021. **210**: p. 1-29.
28. Xu, K., *Tailoring electrolyte composition for LiBOB*. Journal of The Electrochemical Society, 2008. **155**(10): p. A733-A738.
29. Chen, Z.H., et al., *New class of nonaqueous electrolytes for long-life and safe lithium-ion batteries*. Nature Communications, 2013. **4**: p. 1-8.
30. Xu, C., et al., *Experimental study on thermal runaway propagation of lithium-ion battery modules with different parallel-series hybrid connections*. Journal of Cleaner Production, 2021. **284**(124749): p. 1-13.
31. Xing, J. and P. Wu, *State of Charge Estimation of Lithium-Ion Battery Based on Improved Adaptive Unscented Kalman Filter*. Sustainability, 2021. **13**(9): p. 1-16.
32. Xie, Y., et al., *Improving the Air-Cooling Performance for Battery Packs via Electrothermal Modeling and Particle Swarm Optimization*. IEEE Transactions on Transportation Electrification, 2021. **7**(3): p. 1285-1302.
33. Yao, Y.X., et al., *Regulating Interfacial Chemistry in Lithium-Ion Batteries by a Weakly Solvating Electrolyte\*\**. Angewandte Chemie International Edition, 2021. **60**(8): p. 4090-4097.
34. Xie, S.B., et al., *Battery sizing for plug-in hybrid electric buses considering variable route lengths*. Energy, 2021. **226**(7): p. 1-13.
35. Smart, M.C., et al., *Lithium-Ion Electrolytes Containing Ester Cosolvents for Improved Low Temperature Performance*. Journal of The Electrochemical Society, 2010. **157**(12): p. A1361-A1374.
36. Hu, L.B., Z.C. Zhang, and K. Amine, *Fluorinated electrolytes for Li-ion battery: An FEC-based electrolyte for high voltage LiNi<sub>0.5</sub>Mn<sub>1.5</sub>O<sub>4</sub>/graphite couple*. Electrochemistry Communications, 2013. **35**: p. 76-79.
37. Yamagiwa, K., et al., *Improved High-Temperature Performance and Surface Chemistry of Graphite/LiMn<sub>2</sub>O<sub>4</sub> Li-Ion Cells by Fluorosilane-Based Electrolyte Additive*. Electrochimica Acta, 2015. **160**: p. 347-356.
38. Xie, S., et al., *Thermal runaway behavior of lithium-ion batteries in different charging states under low pressure*. International Journal of Energy Research, 2021. **45**(4): p. 5795-5805.

39. Lyu, Y.C., et al., *An Overview on the Advances of LiCoO<sub>2</sub> Cathodes for Lithium-Ion Batteries*. *Advanced Energy Materials*, 2021. **11**(2): p. 1-29.
40. Xiao, J.J., et al., *Ultra-high conductive 3D aluminum photonic crystal as sulfur immobilizer for high-performance lithium-sulfur batteries*. *Nano Research*, 2021. **14**(12): p. 4776-4782.
41. Park, B.C., et al., *Improvement of electrochemical performance of Li[Ni<sub>0.8</sub>Co<sub>0.15</sub>Al<sub>0.05</sub>]O<sub>2</sub> cathode materials by AlF<sub>3</sub> coating at various temperatures*. *Industrial & Engineering Chemistry Research*, 2008. **47**(11): p. 3876-3882.
42. Chen, S., et al., *Synergistic Effects of Stabilizing the Surface Structure and Lowering the Interface Resistance in Improving the Low-Temperature Performances of Layered Lithium-Rich Materials*. *ACS Applied Materials & Interfaces*, 2017. **9**(10): p. 8641-8648.
43. Xiao, F., et al., *State of charge estimation for lithium-ion battery based on Gaussian process regression with deep recurrent kernel*. *International Journal of Electrical Power & Energy Systems*, 2021. **124**: p. 1-15.
44. Nobili, F., et al., *Low-temperature behavior of graphite-tin composite anodes for Li-ion batteries*. *Journal of Power Sources*, 2010. **195**(20): p. 7090-7097.
45. Hou, J.B., et al., *Fundamentals and Challenges of Lithium Ion Batteries at Temperatures between -40 and 60 degrees C*. *Advanced Energy Materials*, 2020. **10**(18).
46. Nobili, F., et al., *Metal-oxidized graphite composite electrodes for lithium-ion batteries*. *Electrochimica Acta*, 2005. **51**(3): p. 536-544.
47. Wei, Z.B., et al., *Load Current and State-of-Charge Coestimation for Current Sensor-Free Lithium-Ion Battery*. *IEEE Transactions on Power Electronics*, 2021. **36**(10): p. 10970-10975.
48. Nobili, F., et al., *High-performance Sn@carbon nanocomposite anode for lithium-ion batteries: Lithium storage processes characterization and low-temperature behavior*. *Electrochimica Acta*, 2013. **107**: p. 85-92.
49. Zhang, S.S., K. Xu, and T.R. Jow, *Electrochemical impedance study on the low temperature of Li-ion batteries*. *Electrochimica Acta*, 2004. **49**(7): p. 1057-1061.
50. Wei, Z.B., et al., *Noise-Immune Model Identification and State-of-Charge Estimation for Lithium-Ion Battery Using Bilinear Parameterization*. *IEEE Transactions on Industrial Electronics*, 2021. **68**(1): p. 312-323.
51. Wang, Z., Q. Ma, and Y. Guo, *Remaining Useful Life Prediction of Lithium-Ion Batteries Based on Deep Learning and Soft Sensing*. *Actuators*, 2021. **10**(9): p. 1-13.
52. Wei, Y.P. and D.Z. Wu, *Prediction of state of health and remaining useful life of lithium-ion battery using graph convolutional network with dual attention mechanisms*. *Reliability Engineering & System Safety*, 2023. **230**: p. 1-11.
53. Bai, G.X., et al., *Prognostics of Lithium-Ion batteries using knowledge-constrained machine learning and Kalman filtering*. *Reliability Engineering & System Safety*, 2023. **231**: p. 1-15.
54. You, H., et al., *Charging Strategy Optimization at Low Temperatures for Li-Ion Batteries Based on Multi-Factor Coupling Aging Model*. *IEEE Transactions on Vehicular Technology*, 2021. **70**(11): p. 11433-11445.
55. Yetik, O., N. Yilmaz, and T.H. Karakoc, *Computational modeling of a lithium-ion battery thermal management system with Al<sub>2</sub>O<sub>3</sub>-based nanofluids*. *International Journal of Energy Research*, 2021. **45**(9): p. 1-12.
56. Yang, Y., et al., *Carbon oxides emissions from lithium-ion batteries under thermal runaway from measurements and predictive model*. *Journal of Energy Storage*, 2021. **33**: p. 1-10.
57. Zhou, Y.P., M.H. Huang, and M. Pecht, *Remaining useful life estimation of lithium-ion cells based on k-nearest neighbor regression with differential evolution optimization*. *Journal of Cleaner Production*, 2020. **249**: p. 1-12.
58. Zhou, D., et al., *Research on online estimation of available capacity of lithium batteries based on daily charging data*. *Journal of Power Sources*, 2020. **451**(227713): p. 1-16.
59. Nagulapati, V.M., et al., *Capacity estimation of batteries: Influence of training dataset size and diversity on data driven prognostic models*. *Reliability Engineering & System Safety*, 2021. **216**: p. 1-11.
60. Chen, L., et al., *Remaining Useful Life Prediction of Battery Using a Novel Indicator and Framework With Fractional Grey Model and Unscented Particle Filter*. *IEEE Transactions on Power Electronics*, 2020. **35**(6): p. 5850-5859.
61. Li, X.Y., C.G. Yuan, and Z.P. Wang, *Multi-time-scale framework for prognostic health condition of lithium battery using modified Gaussian process regression and nonlinear regression*. *Journal of Power Sources*, 2020. **467**(228358): p. 1-12.
62. Wu, J., et al., *Battery-Involved Energy Management for Hybrid Electric Bus Based on Expert-Assistance Deep Deterministic Policy Gradient Algorithm*. *IEEE Transactions on Vehicular Technology*, 2020. **69**(11): p. 12786-12796.

63. Lin, C.-P., et al., *Battery state of health modeling and remaining useful life prediction through time series model*. Applied Energy, 2020. **275**(115338): p. 1-21.
64. Li, P., et al., *State-of-health estimation and remaining useful life prediction for the lithium-ion battery based on a variant long short term memory neural network*. Journal of Power Sources, 2020. **459**(228069): p. 1-12.
65. Wang, S.L., et al., *Improved anti-noise adaptive long short-term memory neural network modeling for the robust remaining useful life prediction of lithium-ion batteries*. Reliability Engineering & System Safety, 2023. **230**: p. 1-12.
66. Lin, M.Q., et al., *Battery health prognosis with gated recurrent unit neural networks and hidden Markov model considering uncertainty quantification*. Reliability Engineering & System Safety, 2023. **230**: p. 1-12.
67. Yang, R., et al., *Characterization of external short circuit faults in electric vehicle Li-ion battery packs and prediction using artificial neural networks*. Applied Energy, 2020. **260**(114253): p. 1-10.
68. Ma, Y., et al., *The capacity estimation and cycle life prediction of lithium-ion batteries using a new broad extreme learning machine approach*. Journal of Power Sources, 2020. **476**(228581): p. 1-11.
69. Ma, Y., et al., *Multiple health indicators fusion-based health prognostic for lithium-ion battery using transfer learning and hybrid deep learning method*. Reliability Engineering & System Safety, 2023. **229**: p. 1-12.
70. Chegade, A.A. and A.A. Hussein, *A Collaborative Gaussian Process Regression Model for Transfer Learning of Capacity Trends Between Li-Ion Battery Cells*. IEEE Transactions on Vehicular Technology, 2020. **69**(9): p. 9542-9552.

## CRedit author statement

**Shunli Wang:** Conceptualization, Methodology, Software.

**Fan Wu:** Visualization, Investigation.

**Paul Takyi-Aninakwa:** Software, Validation.

**Carlos Fernandez:** Data curation, Writing, and Original draft preparation.

**Daniel-Ioan Stroe:** Writing- Reviewing and Editing.

**Qi Huang:** Visualization, Investigation, Supervision.